

Review

Raman scattering as a probe of intermediate phases in glassy networks

P. Boolchand,* Mingji Jin, D. I. Novita and S. Chakravarty

Department of Electrical and Computer Engineering and Computer Science, University of Cincinnati, Cincinnati, OH 45221-0030, USA

Received 1 August 2006; Accepted 22 December 2006

Bulk glass formation occurs over a very small part of phase space, and 'good' glasses (which form even at low quench rates ~ 10 K/sec) select an even smaller part of that accessible phase space. An axiomatic theory provides the physical basis of glass formation, and identifies these sweet spots of glass formation with existence of rigid but stress-free networks for which experimental evidence is rapidly emerging. Recently, theory and experiment have come together to show that these sweet spots of glass formation occur over a range of chemical compositions identified as 'intermediate phases' (IPs). These ranges appear to be controlled by elements of local and medium-range molecular structures that form isostatically rigid networks. IP glasses possess nonhysteretic glass transitions (T_g 's) that do not age much. Raman scattering has played a pivotal role in elucidating the molecular structure of glasses in general, and in identifying domains of IPs. Experiments reveal that these phases possess sharp phase boundaries and are characterized by an optical elasticity that varies with network mean coordination number, r , as power law. In this review, we provide examples in chalcogenide and oxide glass systems in which these phases along with optical elasticity power laws have been established. IP glasses represent self-organized nanostructured functional materials optimized by nature. Copyright © 2007 John Wiley & Sons, Ltd.

KEYWORDS: self-organization in glasses; percolation of rigidity; reversibility window; intermediate phases; Raman scattering; photocontraction

INTRODUCTION

Most liquids upon cooling undergo a first-order transition at the melting point T_m to a crystalline state. On the other hand, select liquids can be supercooled to bypass crystallization and form a glass at a lower temperature called the glass transition temperature,¹ $T_g \approx 2/3$ of T_m . What is so special about these select liquids that readily form glasses? They usually consist of polymeric networks with a mean coordination number $r \sim 2.40$. The quantity r is formally defined as $(1/N)\sum n_i r_i$, where n_i represents the number of atoms having a coordination r_i and $N = \sum n_i$ gives the total number of atoms in a network. The optimum value of $r = 2.40$ was first introduced from an axiomatic theory of glass formation² and has found much support in covalently bonded systems.³ Experiments reveal that space-filling, rigid but unstressed networks do indeed occur near

$r \sim 2.40$. In the past decade, the recognition has emerged^{4–9} that instead of there being a solitary chemical composition,² there is a range of chemical compositions across which the optimal requirement is fulfilled in real glasses. In this special range, also called the *intermediate phase* (IP), not only is the glass-forming tendency optimized but local and intermediate-range structures also give rise to networks that are isostatically rigid. Window glass,¹⁰ thin-film gate dielectrics¹¹ and thermally reversible folding pathways of proteins¹² include some examples of disordered systems in which IPs are manifested.¹³ The starting point to understand IPs is to examine the elastic response of glassy networks.

INTERMEDIATE PHASES IN GLASSY NETWORKS

In 1788, J. L. Lagrange laid the foundations¹⁴ of generalized coordinates and constraints in mechanics in the celebrated book 'Mechanique Analytique'. A century later, J. C. Maxwell showed¹⁵ how these ideas on constraints can be used to understand the mechanical stability of macroscopic

*Correspondence to: P. Boolchand, Department of Electrical and Computer Engineering and Computer Science, University of Cincinnati, Cincinnati, OH 45221-0030, USA.
E-mail: pboolcha@eccecs.uc.edu

structures such as trusses and bridges. More recently, and quite independently, ideas on mechanical constraints were extended to disordered, covalently bonded atomic networks by J. C. Phillips² to understand their glass-forming tendency. He suggested, that the glass-forming tendency is optimized in structures that are optimally constrained, i.e. when

$$n_c = 3 \quad (1)$$

Here n_c represents the mean count of bond-stretching and bond-bending constraints per atom; the network becomes ideally connected in the sense mentioned in the Introduction when the count equals 3, the number of degrees of freedom per atom in 3D. The axiom (1) selects structures that are neither highly nor weakly cross-linked, and leads to the magic connectivity of $r = 2.40$ in percolating networks with no dead ends. Thorpe showed¹⁶ that axiom (1) actually represents a condition for a floppy network to become mechanically rigid. A normal mode analysis of a weakly cross-linked chain network shows cyclical (or floppy) modes (zeros of the dynamical matrix) to a number on average, $f = 3 - n_c$. The values of the average coordination number r (or constraints n_c) per atom are known as the *mean-field* values. In a network of long chains, such as found in a Se glass for example, every atom has two nearest neighbors ($r = 2$), and there is one bond-stretching and one bond-bending constraint per atom. This gives $n_c = 2$ constraints/atom; so there is one floppy mode per atom, $f = 1$. In other words, one-third of the vibrational modes are floppy. Inelastic neutron scattering measurements¹⁷ show a mode near 5 cm^{-1} , which carries one-third of the spectral weight in a Se glass. The presence of floppy modes renders this inorganic polymer network to be rather flexible. Cross-linking the chains of Se by alloying either a group IV and/or a group V additive steadily lowers the floppy mode fraction and, within a mean-field description,^{2,16} the count vanishes linearly as r increases to a critical value $r_c = 2.40$. This defines the elastic phase boundary between a flexible and a rigid network. The mean-field prediction on percolation of rigidity near $r = 2.40$ has been refined in numerical experiments on simple random networks¹⁸ constrained by bond-stretching and bond-bending forces. At $r > 2.40$, one has a stressed-rigid network in which these numerical experiments^{18,19} show shear, longitudinal and transverse elastic constants (C) to increase as a power law in r , i.e.

$$C - C_0 = K(r - r_c)^p \quad (2)$$

with a power p close^{18,19} to 1.50. Here C_0 represents the value of C at $r = r_c$. More recently, numerical experiments have been extended to self-organizing networks of carbon or silicon.²⁰ They show the presence of *two* elastic phase transitions, a *rigidity* transition (r_1), followed by a *stress* transition (r_2). In the intervening region, $r_1 < r < r_2$, the network is rigid but unstressed. This region is an IP

distinguished from the *flexible phase* at $r < r_1$ and the *stressed-rigid phase* at $r > r_2$. In the IP, inserting a new cross-link finds it way to the flexible part of a network, thereby self-organizing it and avoiding forming redundant bonds. The avoidance²⁰ of redundant bonds by reconnecting the network is no longer possible once $r > r_2$. The absence of redundant bonds in the IP ($r_1 < r < r_2$) lowers the free energy, and is the driving force for disordered networks to self-organize. However, the calculated IP widths in amorphous carbon or silicon are much too narrow ($\Delta r = 0.016$),²¹ and the IP centroids always reside at values of r slightly < 2.40 . However, IP widths close to experimental ($\Delta r = 0.12$) values²² have been found in an analytic calculation of realistic alloy structures using a procedure called *size increasing cluster agglomeration* (SICA).²³

A point of current interest relates to aspects of local and intermediate-range structural order that control widths and centroids of IPs in glasses. Rigidity in glassy networks can be traced to rings that have typically four to six atoms.^{21,23} Larger rings tend to be flexible while the smaller ones are stressed-rigid. The relevant scale of molecular structures is therefore typically 10 \AA in size. However, the way rings connect to each other forming a network of superstructure of rings is also relevant. IPs are non-mean-field phases of glassy networks in that more than the closest environment of individual atoms is relevant; and their detection in experiments requires methods that, in general, probe a network at all length scales. Recently, IPs have been found in numerical simulations on triangular networks,^{24,25} and the suggestion has been made²⁵ that IPs may be manifestations of self-organized criticality.

EXPERIMENTAL PROBES OF INTERMEDIATE PHASES

The breakdown of the $k = 0$ selection rule²⁶ in disordered systems, permits Raman scattering^{27,28} to be a particularly fertile probe of *local* ($\sim 3 \text{ \AA}$) and *intermediate-range* ($\sim 10 \text{ \AA}$) structures of glassy networks. In some cases these experiments have been an avenue to establish the *three* elastic phases in glasses as discussed earlier.⁴⁻⁷ When a vibrational mode forms part of a network and has some extended character, one can experimentally define optical elastic power laws, such as in Eqn (2), from variations in the mode frequency (ν) as a function of network connectivity r .

$$\nu^2 - \nu_c^2 = K(r - r_c)^p \quad (3)$$

Here ν_c represents the value of ν at the elastic threshold r_c . Several binary and ternary covalent glass systems have been examined in this respect, and the results show⁴⁻⁷ the elastic power law in the IPs and stressed-rigid phases to be $p \sim 1.0$ and ~ 1.5 , respectively. Thus, Raman scattering through a measurement of optic modes as a function of network connectivity has permitted probing glassy networks not only at a local scale but also at intermediate and even extended length scales. We shall return to discuss this point in conjunction with experimental results later.

When a crystalline solid is squeezed by the application of a hydrostatic pressure P , the bonds reduce in length and vibrational modes, in general, blue shift on account of the anharmonicity of bonds.²⁹ In glasses, parallel experiments have demonstrated that the vibrational modes usually broaden and also blue shift, but only when the external pressure (P) exceeds a threshold value (P_c). P_c is generally regarded³⁰ as a measure of network internal stress in a glass, and the external pressure P must exceed P_c for a glassy network to *feel* the applied pressure. Recent Raman pressure experiments on the binary $\text{Ge}_x\text{Se}_{1-x}$ glasses have shown²² trends in threshold pressures, $P_c(x)$, which vanishes in IP compositions $0.20 < x < 0.25$ and increases steadily once $x > 0.25$ in the stressed-rigid phase or when $x < 0.20$ in the flexible phase. Thus, Raman scattering through pressure measurements using diamond anvil cells has also served as a useful probe of network stress in glasses in general, and IPs in particular.

Brillouin scattering is a powerful probe of acoustic excitations in solids³¹ including glasses. In such experiments the intrinsic length scale to which a glassy network is probed is set by the wavelength of a longitudinal or a transverse acoustic excitation, which typically lies in the range of 100 nm or larger in oxide and chalcogenide glasses.³² Since this length scale exceeds the relevant length scale of ring (~ 10 Å) structural order in IPs, Brillouin scattering largely serves as a mean-field probe of elastic behavior in glasses.³² On the other hand, Raman scattering through optic modes can probe glass structure at both short and extended ranges to detect IPs. For these reasons, IPs are manifested in Raman scattering⁸ but not in Brillouin scattering^{32,33} experiments.

A particularly rewarding probe of elastic phases in glasses is *modulated differential scanning calorimetry* (m-DSC).^{34–36} The thermal probe permits a detailed examination of a glass transition endotherm using in essence AC calorimetry.³⁴ In AC calorimetry, one applies a small sinusoidal heat flux and measures the temperature response at the same frequency, permitting the frequency dependence of the specific heat to be established. In m-DSC, one superposes a sinusoidal temperature variation over a linear temperature ramp to thermally scan across a glass transition, and deconvolutes the *total* heat flow endotherm near a glass transition into two contributions:^{35,36} one that tracks the sinusoidal variations and is called the *reversing* heat flow, and the other the difference signal between the *total* and *reversing* heat flow that does not track the temperature oscillations and it is reckoned as the *nonreversing* component of heat flow. The reversing heat flow usually shows a step typically from 20 to 40 °C wide, and one defines the glass transition temperature (T_g) by the inflexion point of the step. The step height gives the specific heat change across the glass transition. The much higher sensitivity of the AC (m-DSC) over the traditional DC measurements (DSC) has the advantage that one can use much lower scan rates in the former (2 °C/min) compared to the latter (20 °C/min).

The m-DSC method permits obtaining scan rate and thermal history independent T_g 's. The nonreversing heat flow usually shows a Gaussian-like profile as a precursor to the glass transition, and the frequency-corrected^{35,36} area under the Gaussian profile provides a quantitative measure of the nonreversing enthalpy (ΔH_{nr}) of the glass transition. Experiments on a variety of glasses have revealed compositional windows across which the ΔH_{nr} term nearly vanishes,^{4,22} and glass transitions become thermally reversing (reversibility window) in character.³⁶ Glass systems examined in both Raman scattering and m-DSC experiments reveal the rather spectacular result that the IPs inferred in Raman scattering virtually coincide with thermal reversibility windows. In retrospect this is not surprising given the fact that both the thermal and optical method probe glassy networks at all length scales. The correlation between the thermal and the optical probe of IPs has served as an independent check of one method over the other, and together both techniques have provided new insights into the elusive nature of glass transitions^{4,37} and self-organization¹³ in disordered systems.

INTERMEDIATE PHASES IN CHALCOGENIDE GLASSES

Binary and ternary alloys of the group IV (Si, Ge, Sn) and group V (P, As, Sb) with the group VI (S, Se and Te) elements (chalcogens) represent some of the best glass formers in nature. These chalcogenide alloy glasses are easily synthesized by reacting the pure elements. Starting from a pure Se glass, the addition of a group IV and/or a group V element leads to a progressive cross-link of the selenium chain network to increase its mean coordination number r . This behavior is reflected in compositional trends of $T_g(r)$ for which theoretical support has emerged from stochastic agglomeration theory.³⁸

Consider the cases of binary $\text{Ge}_x\text{Se}_{1-x}$, $\text{P}_x\text{Se}_{1-x}$ and ternary $\text{Ge}_y\text{P}_y\text{Se}_{1-2y}$ glasses for which the compositional trends³⁹ in T_g appear in Fig. 1. One observes thresholds in T_g for the case of the two binary glass systems near their chemical thresholds ($r_t = 2.67$ and 2.40), but the absence of such a threshold in the ternary glass system near the chemical threshold ($r_t = 2.55$). The chemical threshold represents the glass chemical composition at which the available Se is all used up in forming the Ge- and P-centered local structures, thereby leaving no excess Se in the network to form Se_n chain fragments. In the ternary glass system, the chemical threshold occurs⁶ at $x_t = 18.18\%$ corresponding to $r_t = 2.55$. In binary glasses, once r approaches r_t , in many instances the cation–cation bonds formed are found to intrinsically segregate from the backbone leading to nanoscale phase separation (NSPS) of glasses. Specifically, in binary $\text{Ge}_x\text{Se}_{1-x}$ glasses, Ge–Ge bonds and in $\text{P}_x\text{Se}_{1-x}$ glasses, P–P bonds, apparently demix from the backbone to form nanophases at $r > r_t$. The loss in network connectivity on account of NSPS in glasses leads to global maxima in T_g near chemical

thresholds,⁴⁰ and is reminiscent of a parallel behavior of the liquids of the corresponding crystals in the equilibrium phase diagrams. These NSPS effects are qualitatively absent³⁹ in the ternary glass system, demonstrating that Ge–Ge bonds and P–P bonds formed at $r > r_t$ largely form as part of the backbone. In a similar fashion, the case of $\text{Ge}_x\text{As}_x\text{Se}_{1-2x}$ ternary has been extensively investigated.^{6,8} Ternary glasses are particularly attractive systems to examine connectivity-related phase transitions because of the absence of NSPS effects.³⁹

The richness of the Raman scattering results in ternary glasses⁴¹ is displayed in Fig. 2, which gives the observed line-shapes at low, intermediate, high and very high wavenumbers in four separate panels. The spectra are stacked bottom up with increasing content of P or Ge, and mode identification is provided in Table 1 and the labels in Fig. 2. These spectra provide a pictorial view of glass molecular structure evolution with x , and the principal features are as follows. At $x = 0$, one starts with a Se_n chain glass with a finite concentration of Se_8 rings.⁴² Addition of Ge and P ($x = 3\%$) leads to the formation of Ge-centered corner-sharing (CS) and edge-sharing (ES) tetrahedra,^{43,44} and P-centered pyramidal (PYR) and quasitetrahedral (QT) units⁴⁵ that serve to cross-link the chains of Se_n . Polymeric ethylene-like P_2Se_4 units containing P–P bonds are first manifested⁴⁵ near $x \sim 9\%$ and grow rapidly with x . Near $x \sim 20\%$, P_4Se_3 molecules are formed,^{45,46} which decouple from the backbone in the $18\% < x < 24\%$ range (NSPS) from the backbone. At higher x , a variety of new structures form, including ethane-like

Ge_2Se_6 , amorphous Ge,⁴⁷ amorphous phosphorus⁴⁸ and P_4 monomers.^{49,50}

The feature of principal interest in the Raman spectra of Fig. 2 is the CS mode of GeSe_4 tetrahedra⁴³ near 200 cm^{-1} . The mode wavenumber is found to steadily blue shift as a function of x , a behavior that is mapped in Figs 2(b) and 3(b). At low x ($< 5\%$) and in region I, glasses age ever so slowly and the mode wavenumber steadily blue shifts in time over a period of months, a feature that is characteristic of flexible glasses. However, as x increases to 7% , such aging is qualitatively suppressed, and variations in mode wavenumber, $\nu_{\text{CS}}(x)$, display a mild kink (change in slope) near $x = 9\%$. The $\nu_{\text{CS}}(x)$ variation is almost linear in the $9\% < x < 14.5\%$ range, (region II in Fig. 3(b)). This is followed by a small jump in wavenumber of about 0.4 cm^{-1} near $x = 14\%$, and a power law variation in region III, $14.55 < x < 17\%$. A mild NSPS of the ternary glass initiates at $x > 18\%$ as P_4Se_3 molecules decouple from the backbone^{45,46} and lower the global connectivity (Fig. 3(a)), interrupting the power law variation, an issue we discuss next.

The nature of the CS mode of a GeSe_4 tetrahedral unit in GeSe_2 glass has been examined in *ab initio* molecular dynamics (MD) simulations,⁵¹ and inverse participation ratios reveal that the mode has some extended character. This is not unexpected given that the Se bridging bond angle across two tetrahedral units deviates from 90° . The structural feature ensures that the motions of adjacent tetrahedra are coupled to each other. Raman scattering through a measurement of the vibrational wavenumber of the mode in question therefore serves as a medium-range and extended-range probe of the elastic behavior of glasses particularly as the Ge concentration increases and the extended regions around each tetrahedral unit begin to overlap. The mode wavenumber squared measured relative to its threshold value, $\nu_{\text{CS}}^2 - \nu_c^2$, provides a measure of the optical elastic constant ($C - C_0$) of the backbone with the constant of proportionality representing the inverse of Ge reduced mass. With increasing x , the backbone progressively cross-links, and its stiffening is reflected in a blue shift of the vibrational mode wavenumber. In region II, the results of Fig. 3(b) show a power law, $p = 0.99(3)$. In region III, results of Fig. 4 yield a power law $p = 1.48(2)$. In the analysis, we have proceeded by fitting these data sets using both log–log plots and, separately, polynomial fits to Eqn (2). By steadily changing the phase boundary values, $x_c(1)$, $x_c(2)$, from an initial estimate, both types of fits converge to give the same value of the power law p as illustrated in Fig. 4.

In the present glasses, once the P (or Ge) concentration x exceeds 18% , our Raman scattering data show some P_4Se_3 molecules to decouple from the backbone (Figs 2(c) and (d)), and in m-DSC experiments a satellite window (Fig. 3(a)) in the ΔH_{nr} term is manifested. These features are associated with a mild NSPS of the ternary glasses. Of interest here is the fact that once the glass demixes, the power law variation (Fig. 3(b)) is interrupted. These data corroborate the view

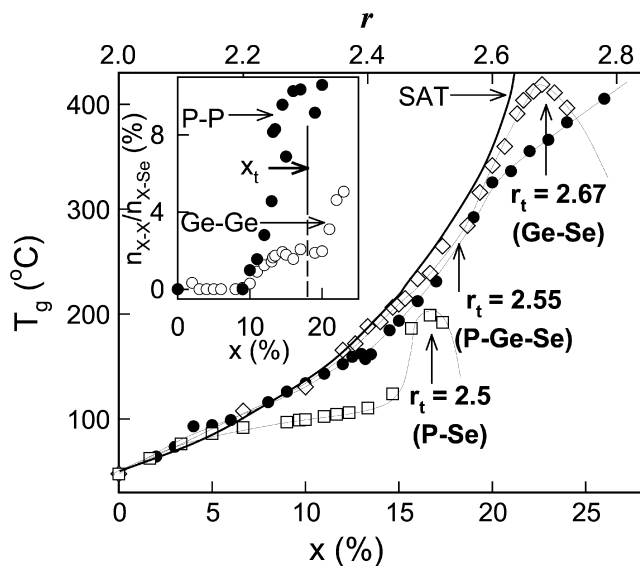


Figure 1. Variations in $T_g(r)$ in binary $\text{Ge}_x\text{Se}_{1-x}$, $\text{P}_x\text{Se}_{1-x}$ and ternary $\text{P}_y\text{Ge}_y\text{Se}_{1-2y}$ glasses. $r = 2(1+x)$ for the $\text{Ge}_x\text{Se}_{1-x}$ system, $r = 2+x$ for the $\text{P}_x\text{Se}_{1-x}$ system and $r = 2+3y$ for the $\text{Ge}_y\text{P}_y\text{Se}_{1-2y}$ ternary. The inset shows the expected variation in the count of homopolar bonds Ge–Ge and P–P in the ternary glasses based on variations in T_g predicted by stochastic agglomeration theory (Taken from Ref. 7).

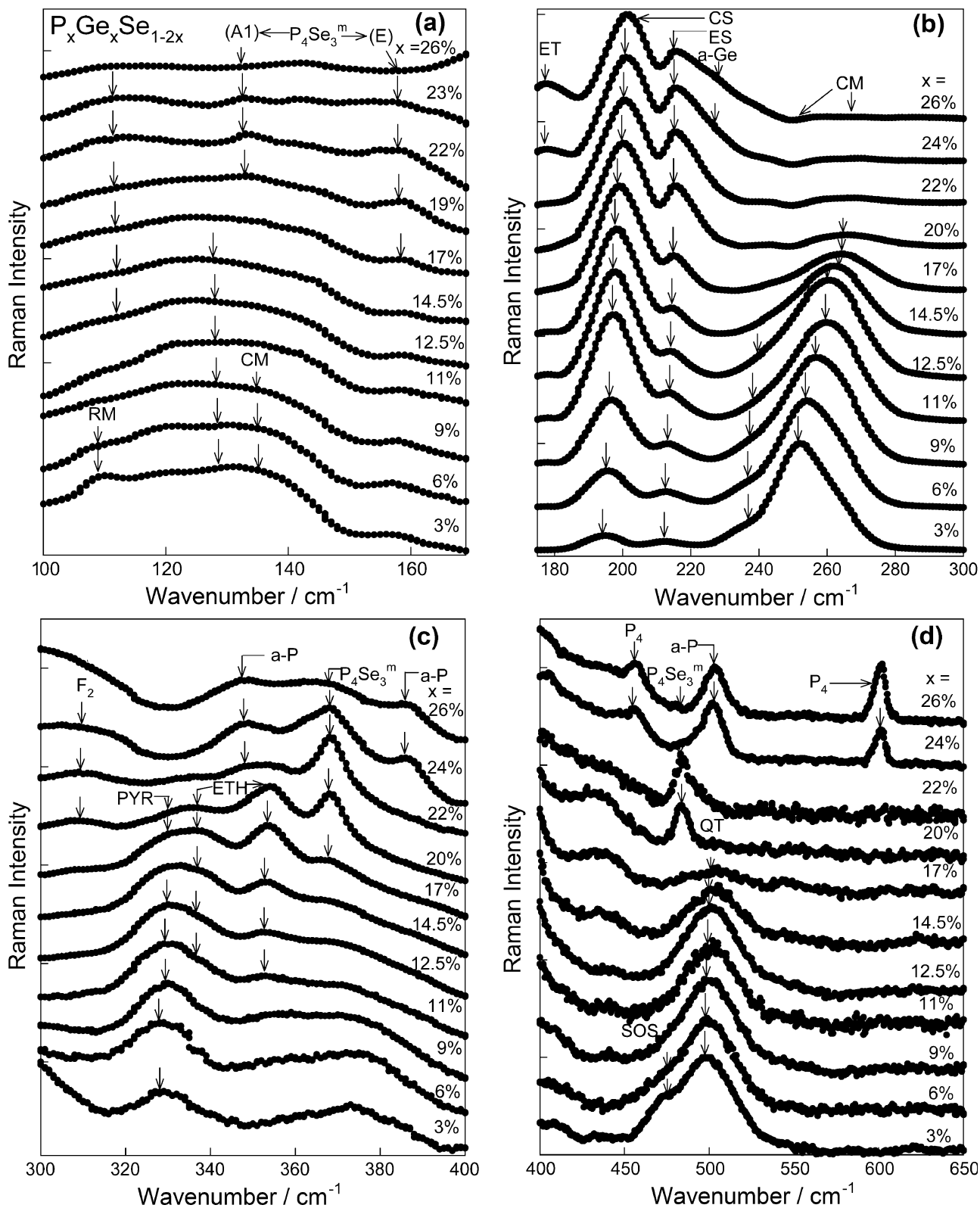


Figure 2. Raman scattering in $P_xGe_xSe_{1-2x}$ glasses excited by $1.06\ \mu\text{m}$ radiation and analyzed using a Thermo-Nicolet Fourier Transform Raman system. Refer Table 1 for the mode assignments. SOS: second-order scattering; QT: quasitetrahedral; PYR: pyramidal; CM: Se chain mode; RM: Se_8 ring mode.

Table 1. Mode labels, mode wavenumber, mode assignment and references for the Raman vibrational modes observed in ternary $\text{Ge}_x\text{P}_x\text{Se}_{1-2x}$ glasses

Mode labels	Mode wavenumber (cm^{-1})	Mode assignment	Reference
CS	198	$\text{Ge}(\text{Se}_{1/2})_4$ corner-sharing tetrahedra	Jackson <i>et al.</i> ⁴³
ES	215	$\text{Ge}(\text{Se}_{1/2})_4$ edge-sharing tetrahedra	Jackson <i>et al.</i> ⁴³
F2	115, 130, 308	$\text{Ge}(\text{Se}_{1/2})_4$ F ₂ mode	Bridenbaugh <i>et al.</i> ⁴⁴
CM, A1 CM, E	237, 256 138	Se_n chain (A_1 mode) Se_n chain (E mode)	Zallen and Lucovsky ⁴²
RM	112	Se_8 rings (A_1 mode)	Zallen and Lucovsky ⁴²
ET	175, 208	$\text{Ge}_2(\text{Se}_{1/2})_6$ ethane-like units	Jackson <i>et al.</i> ⁴³
PYR	210, 330	$\text{P}(\text{Se}_{1/2})_3$ pyramids	Georgiev <i>et al.</i> ⁴⁵
ETH	180, 330, 350, 370	$\text{P}_2(\text{Se}_{1/2})_2\text{Se}_2$ ethylene-like units	Georgiev <i>et al.</i> ⁴⁵
QT	500	$\text{Se} = \text{P}(\text{Se}_{1/2})_3$ quasitetrahedral units	Georgiev <i>et al.</i> ⁴⁵
P_4	363, 465, 606	P_4 clusters	Venkateswaran ⁴⁹ Andreas <i>et al.</i> ⁵⁰
$\text{P}_4\text{Se}_3^{\text{III}}$ A1 $\text{P}_4\text{Se}_3^{\text{III}}$ E	184, 212, 368, 371, 483 135, 165, 425	P_4Se_3 monomers (A_1 mode) P_4Se_3 monomers (E mode)	Verrall <i>et al.</i> , ⁴⁶ Georgiev <i>et al.</i> ⁴⁵
a-P	355, 389, 398, 425, 458, 500	Amorphous P	Lannin <i>et al.</i> ⁴⁸
a-Ge	230	Amorphous Ge	Choi <i>et al.</i> ⁴⁷

that the CS mode wavenumber is, indeed, a good probe of network connectivity as long as the network remains fully polymerized.

The compositional trends in the $\Delta H_{\text{nr}}(x)$ term, inferred from m-DSC experiments are compared to those of the Raman CS mode wavenumber in Fig. 3. The correlation between the reversibility window and region II is quite striking. In the reversibility window glasses are in the IP. In Region III, the elastic power law of $p = 1.48$ (Eqn. 2) is in excellent agreement with the value predicted for stressed-rigid networks in numerical experiments.^{18,19} There are currently no theoretical predictions for the elastic power law in IPs. Raman results on binary ($\text{Si}_x\text{Se}_{1-x}$ glasses⁵ $\text{Ge}_x\text{Se}_{1-x}$ glasses⁸) and ternary ($\text{Ge}_x\text{As}_x\text{Se}_{1-2x}$)⁶ glasses reveal, for elastic power laws in the IP and stressed-rigid phases, values that are quite similar to the ones observed here in the $\text{Ge}_y\text{P}_y\text{Se}_{1-2y}$ ternary. A summary²² of IPs in several chalcogenide glasses appears in Fig. 5 as a bar chart, with the length of the bar delineating the IP-width in r .

Another significant finding of the m-DSC results (Fig. 3) on the present ternary glasses is the aging behavior of the $\Delta H_{\text{nr}}(x)$ term. In these experiments glass samples were aged at room temperature, $T < T_g$, and glass transitions studied for periods up to 6 months after synthesis. We find that the $\Delta H_{\text{nr}}(x)$ term for glass compositions in the flexible and stressed-rigid regimes ages, but such aging is qualitatively absent for IP glass compositions. This is a remarkable feature of IP glasses and has been discussed elsewhere.⁷

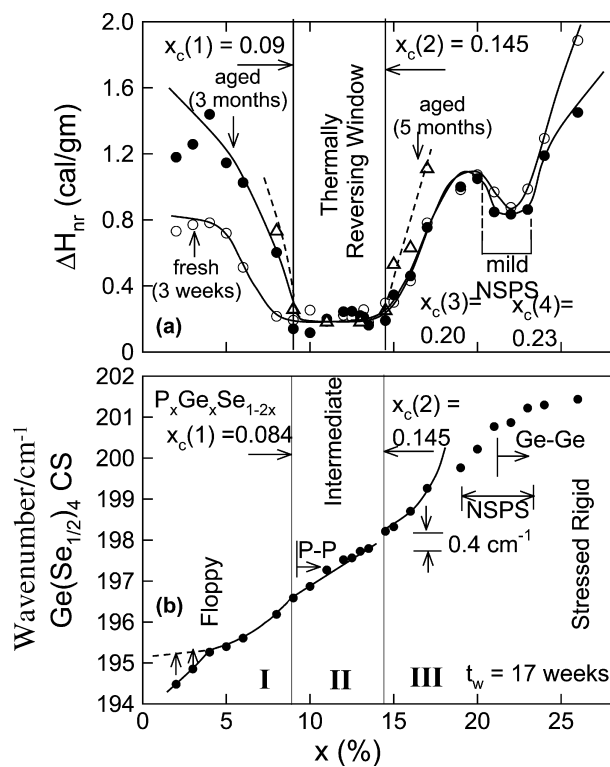


Figure 3. Compositional trends in the nonreversing enthalpy $\Delta H_{\text{nr}}(x)$ of glass transition in the top panel, and trends in Raman CS mode wavenumber in the bottom panel. The thermal and optical experiments reveal elastic phase boundaries that more or less coincide for $\text{P}_x\text{Ge}_x\text{Se}_{1-2x}$ glasses.

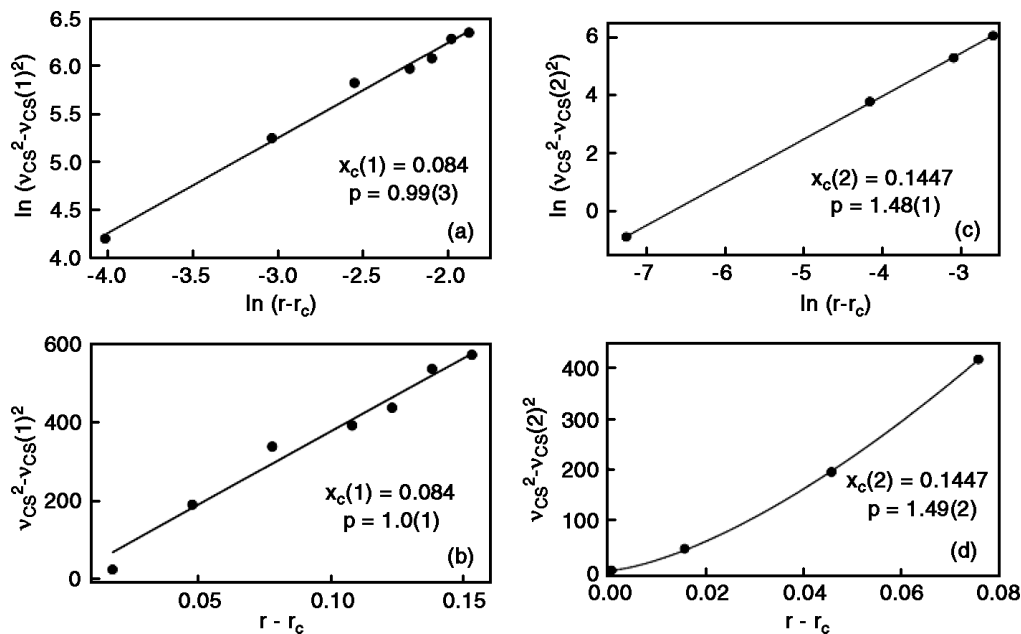


Figure 4. Power law (top) and polynomial fits (bottom) to the CS mode wavenumber squared in the IP (left panels) and the stressed-rigid phase (right panels) to deduce the elasticity power laws in ternary $\text{Ge}_x\text{P}_x\text{Se}_{1-2x}$ bulk glasses.

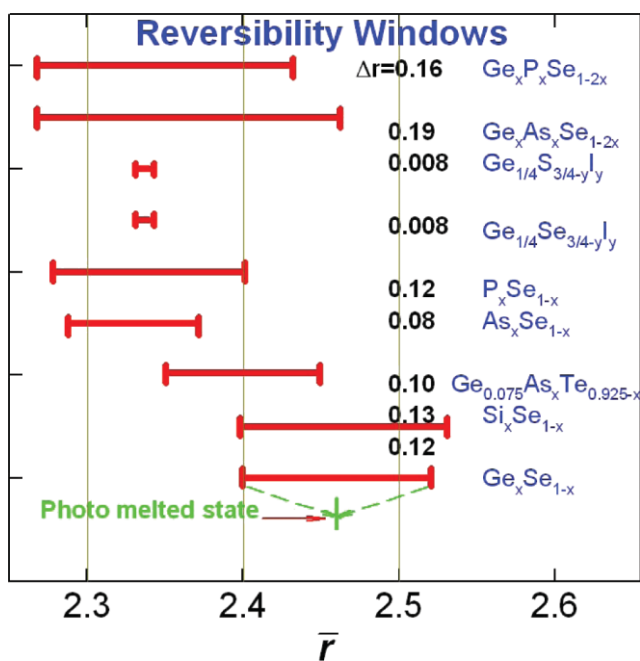


Figure 5. Observed intermediate phase widths (length of the solid line) in r -space for the indicated binary and ternary chalcogenide glasses. This figure is available in colour online at www.interscience.wiley.com/journal/jrs.

Trends in IP widths of several covalent glasses are summarized in Fig. 5. We note that, in general, group V selenides have IPs that lie below $r < 2.40$ while the group IV selenides have IPs that lie at $r > 2.40$. Ternary glasses of both group

IV and V selenides have IPs that are much wider, and generally encompass the previous two ranges characteristic of the group IV and V selenides. On the other hand, IPs in chalcogenide are found to be extremely narrow,^{9,52} probably because halogen atoms serve to scission chalcogen bridges and break characteristic rings where rigidity is nucleated.

What is so special about these IPs? These networks are usually composed of local and medium-range structures that are isostatically rigid, i.e. that are rigid but with no redundant bonds (that create stress). In ternary $\text{Ge}_x\text{P}_x\text{Se}_{1-2x}$ glasses, the isotactic local structures populated⁷ in the IP include CS GeSe_4 tetrahedra ($r = 2.40$), pyramidal $\text{P}(\text{Se}_{1/2})_3$ units ($r = 2.40$) and quasitrahedrally coordinated $\text{Se} = \text{P}(\text{Se}_{1/2})_3$ units ($r = 2.28$). For each of these units, the count of constraints due to bond-stretching and bond-bending forces per atom yields, $n_c = 3$, even though their mean coordination numbers r (indicated in parenthesis) change as reflected by their chemical stoichiometries. Raman pressure experiments²² on glasses have shown that networks in IPs are stress free and that in the flexible and the stressed-rigid elastic phases have internal stresses. IP glasses exist in a state of quasiequilibrium by virtue of an ideal connectivity at all length scales,²¹ which is largely driven by these systems lowering their free energy by expelling redundant bonds. The absence of aging in IP glasses is a manifestation of the quasiequilibrium of the network structure. Thus, even though IP glassy networks are disordered, in so far as network stress is concerned, they behave much like crystalline solids. The reversibility of the glass transition and its nonaging characteristic for IP glass compositions capture the basic principles that underlie self-organization of disordered networks.

GIANT PHOTOCONTRACTION (PC) OF OBLIQUELY DEPOSITED $\text{Ge}_x\text{Se}_{1-x}$ THIN FILMS AND INTERMEDIATE PHASES

The binary $\text{Ge}_x\text{Se}_{1-x}$ glass system was one of the first in which existence of the IP was established.⁸ It spans the $0.20 < x \ll 0.25$ range as shown in Fig. 6. In the 1980s, Chopra *et al.*⁵³ showed that obliquely deposited $\text{Ge}_x\text{Se}_{1-x}$ thin films are porous and possess a columnar structure. When such films (typical thickness $t \sim 1 \mu\text{m}$) are irradiated by a Hg-vapor lamp, they undergo a contraction with fractional changes in thickness ($\Delta t/t$) of as much as 25%. Thin films of the Ge-As-Se ternary⁵⁴ showed a rather large photocontraction (PC) effect of nearly 25% near a mean coordination of $r \sim 2.40$. The growth of columns in obliquely deposited films is not unique to amorphous chalcogenides, but the giant PC of such films after exposure to super-band-gap light certainly is. The molecular origin of this giant PC effect has remained largely speculative⁵⁵ to date.

We have recently re-examined obliquely deposited thin films of $\text{Ge}_x\text{Se}_{1-x}$ over a wide composition range x ($0.15 < x < 0.33$). The films were synthesized in Professor Chopra's laboratory at the Indian Institute of Technology, New Delhi, using an experimental setup in which thin films at five oblique angles ($\alpha = 0, 20, 45, 60$ and 80°) were deposited simultaneously using one evaporation charge. Si wafers and glass slides were used as substrates and film thicknesses were in the $1\text{--}2 \mu\text{m}$ range. In all cases, the evaporation charges used were the corresponding bulk glasses that were characterized by Raman scattering. Films were examined in SEM, Raman scattering, IR reflectance, and profilometry measurements both in the virgin (as-deposited state) and in the postilluminated state. Films mounted on a cold stage and purged with nitrogen gas were exposed using an

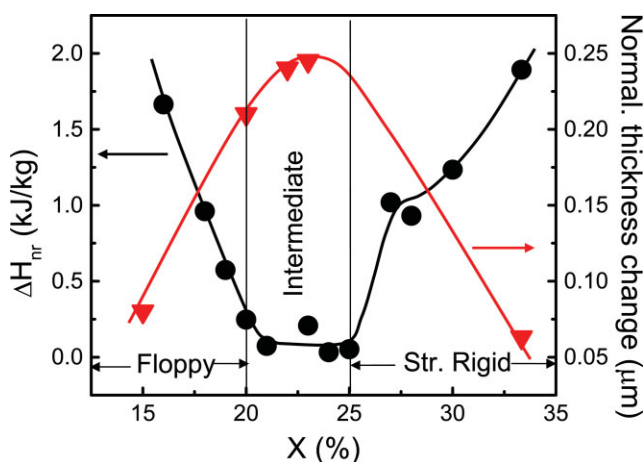


Figure 6. Compositional trends in light-induced contraction of obliquely deposited ($\alpha = 80^\circ$) $\text{Ge}_x\text{Se}_{1-x}$ thin films (\blacktriangledown present work) and the nonreversing enthalpy (\bullet) $\Delta H_{nr}(x)$ in bulk $\text{Ge}_x\text{Se}_{1-x}$ glasses. This figure is available in colour online at www.interscience.wiley.com/journal/jrs.

Hg-Xe-vapor lamp to appropriate integrated doses of visible radiation and the PC observed. Figure 7 shows an SEM image of a GeSe_2 film obliquely deposited at $\alpha = 80^\circ$. The columnar structure is readily observed in the SEM viewgraph. The bottom panel shows a cartoon of the film microstructure, which consists of columns of a phase labeled A, and an intercolumnar phase labeled B. Columns usually grow at an angle β with respect to the film normal when the atomic vapor is directed at an angle of incidence α . Dirk and Leamy have shown⁵⁶ that the angles α and β are related as $\tan \alpha = 2 \tan \beta$.

Figure 6 shows trends in PC of $\text{Ge}_x\text{Se}_{1-x}$ films. It is seen to be largest in the IP. We have also carried out Raman scattering on films as a function of obliqueness angle α at several compositions.

Figure 8 compares the lineshapes of GeSe_2 thin films deposited at three obliqueness angles ($0, 60$ and 80°) with that of the stoichiometric bulk glass used as the evaporation charge. Several features are seen in these results. The film deposited at normal incidence ($\alpha = 0^\circ$) displays vibrational features that are quite similar to those of the bulk glass, thereby serving as a test of the thin film deposition process. Tuning the evaporation parameters is crucial to obtain films

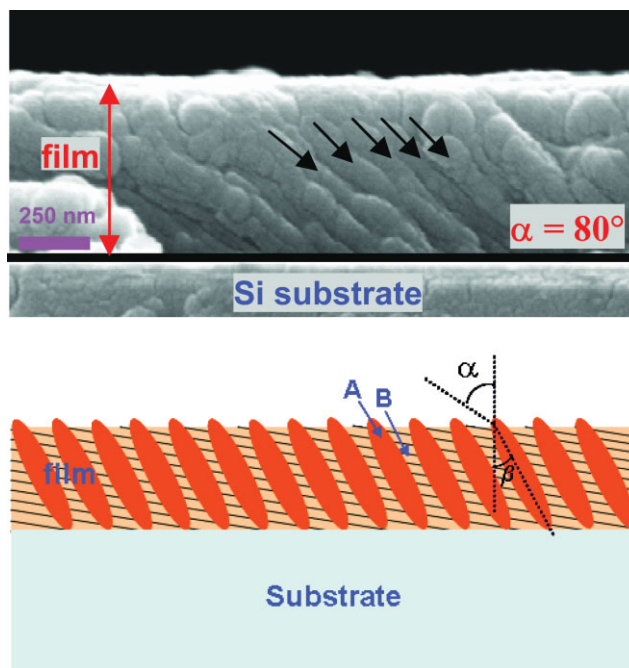


Figure 7. Scanning electron micrograph of an obliquely deposited thin film of GeSe_2 showing the columnar structure (top panel). A schematic model of the film structure is shown in the bottom panel. The obliqueness angle α indicates the angle made by the incident atomic vapor with the thin film normal, while the angle β gives the angle between the column axis and the film normal. A and B designate the column and intercolumnar molecular phases populated in the films. Refer text for details. This figure is available in colour online at www.interscience.wiley.com/journal/jrs.

possessing a molecular structure similar to that of the bulk glass. On the other hand, we find that films deposited at high obliqueness angles (of 60° and 80°) progressively phase-separate into a Ge-rich and a Se-rich phase that can be approximately described by the following stoichiometric relation:



Analysis of the Raman lineshapes⁵⁷ reveals that the stoichiometry of the Se-rich phase is close to $\text{Ge}_{23}\text{Se}_{77}$, while that of the Ge-rich phase close to $\text{Ge}_{42}\text{Se}_{58}$. Since the band gap of the Ge-rich phase (<1.5 eV) is smaller than that of the Se-rich phase (2.0 eV), and particularly since the latter gap is slightly larger than the laser energy (1.9 eV, 647 nm) used, Raman scattering from films is dominated by resonant enhancement of the Se-rich phase. The principal features of the Se-rich phase in obliquely deposited $\alpha = 80^\circ$ films include: (1) presence of Se_n chain mode near 260 cm^{-1} , (2) a red shift of the CS mode and (3) a reduction in scattering strength ratio of the ES to CS mode in relation to the normally deposited film ($\alpha = 0^\circ$) as shown in Fig. 8. These features uniquely fix the stoichiometry⁵⁷ of the Se-rich phase to close to the centroid of the reversibility window (Fig. 6). The principal feature of the Ge-rich phase is a steadily declining scattering strength of the mode near 180 cm^{-1} as α increases to 80° . We identify this with a normal mode of ethane-like Ge_2Se_6 units.⁵⁸ In sharp contrast, Raman scattering results on thin films at $x = 0.23$ (Fig. 9) are found to display lineshapes

that are largely *independent* of obliqueness angle α . This observation suggests that the deposited phase appearing at this composition is the IP, which is rigid but stress free and can easily grow in either columns or as a bulk 3D network.

It appears that two basic phenomena come together for the PC effect to be manifested in the present films. First, the morphological structure of the obliquely deposited ($\alpha = 80^\circ$) thin films consists of two phases: a phase A that undergoes facile photocollapse and a second phase B that does not. Films at $x = 0.23$ consist entirely of the generic A phase, which can exist either in a columnar form or as a 3D network of interlocking rings. Films at $x > 0.25$, such as stoichiometric GeSe_2 , consist both of a phase A (columns) and an intercolumnar Ge-rich phase B, as revealed by Raman scattering (Fig. 8). A parallel situation prevails in films at $x < 0.20$, which segregate into phase A (columns) and an intercolumnar Se-rich phase B. As mentioned earlier, many materials can be obliquely deposited to form columnar structures but only the amorphous thin films of the chalcogenides undergo pronounced PC effects. The second crucial feature of chalcogenide glasses is that phase A undergoes facile photomelting. Photomelting of bulk $\text{Ge}_{23}\text{Se}_{77}$ glasses has been observed in micro-Raman scattering experiments as discussed elsewhere.⁸ Super-band-gap radiation leads to switching of covalent bonds by an electronic process that has been described elsewhere⁵⁹ by Fritzsche. The compositional trends in the PC effect illustrated in Fig. 7 follow naturally from these considerations. The PC effect is maximized when only the A-phase is in the reversibility window, $0.20 < x < 0.25$, since it undergoes photomelting and leads to a collapse of the columns. At $x > 0.25$ the intercolumnar Ge-rich phase B grows at the expense of the phase A, and its growth

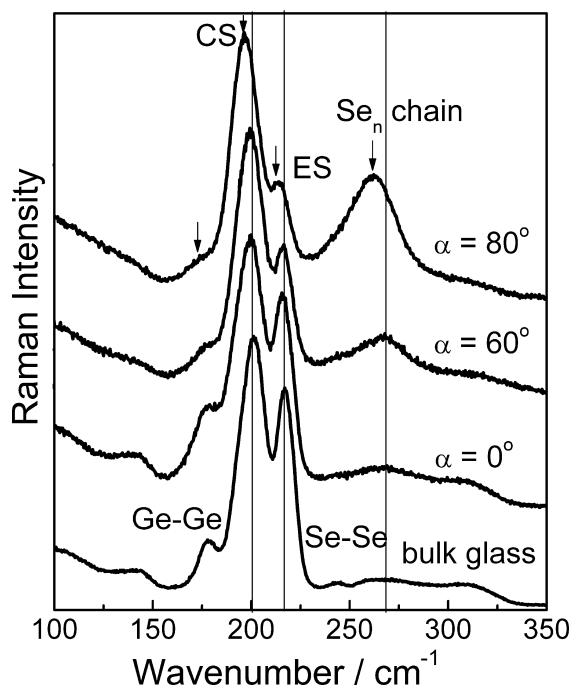


Figure 8. Raman scattering from obliquely deposited GeSe_2 thin films at three angles ($\alpha = 0, 60$ and 80°) compared to that of a bulk glass. The scattering was excited using 647 nm radiation.

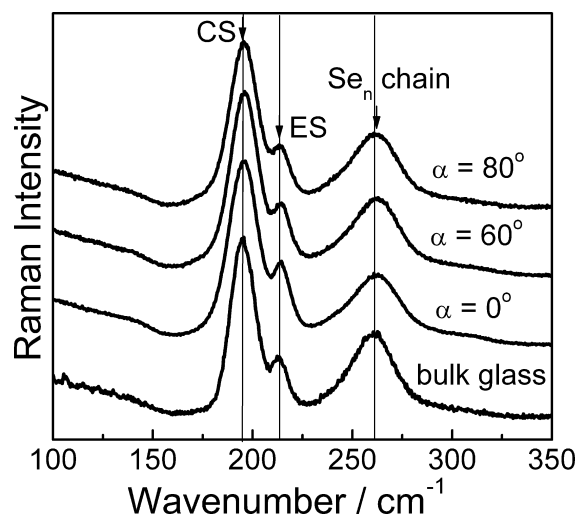


Figure 9. Raman scattering in obliquely deposited $\text{Ge}_{23}\text{Se}_{77}$ thin films at three angles ($\alpha = 0, 60$ and 80°) compared to that of a bulk glass. The scattering was excited using 647 nm radiation.

steadily suppresses the PC effect because it is intrinsically stressed and is not expected to undergo photomelting. Parallel considerations apply to thin films at $x < 0.20$, where growth of the Se-rich B-phase serves to suppress the PC effect (Fig. 6) largely because it is also stressed.²²

The segregation of bulk $\text{Ge}_x\text{Se}_{1-x}$ glasses into two phases A and B upon oblique deposition (Eqn (4) reaction going to the right) can be partially reversed when films are photocontracted upon exposure to Hg-vapor lamp. The chemical bonding or reconstruction of phase A with phase B is supported by Raman scattering. We have examined GeSe_2 thin films after Hg light exposure, and in Fig. 10 compare the observed lineshape of a virgin film with its postilluminated counterpart. The super-band-gap radiation (470 nm, 2.63 eV) from a Hg lamp penetrates only to a small depth in obliquely deposited films. Such is not the case with the 647 nm excitation used to excite Raman scattering, which essentially probes the total film thickness. The reduction in scattering strength of the chain mode near 260 cm^{-1} and the enhancement in scattering strength of the ES mode (216 cm^{-1}), both normalized to the CS mode (200 cm^{-1}), serve to illustrate that some part of the phase separation has been reversed by Hg light exposure. In summary, it appears that the giant PC effect is a manifestation of photomelting of the self-organized columns formed in IP compositions of these obliquely deposited thin films.

INTERMEDIATE PHASES IN SOLID ELECTROLYTE GLASSES

Alloys of base oxide (B_2O_3 , AgPO_3 , GeO_2) or chalcogenide (As_2S_3 , GeSe_4) glasses with solid electrolytes (alkali oxides

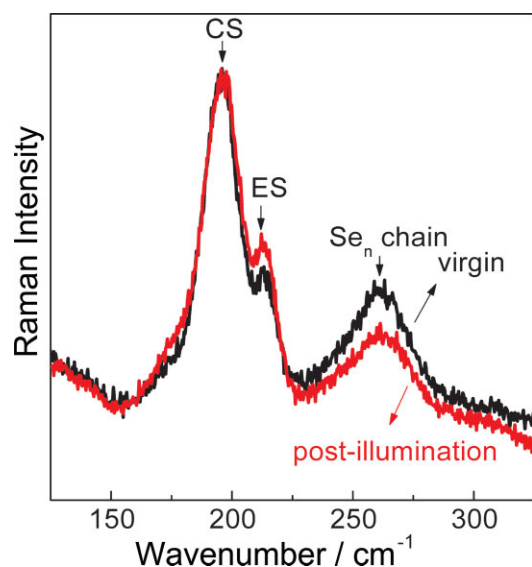


Figure 10. Raman scattering of an obliquely (80°) deposited GeSe_2 thin film taken before and after Hg light irradiation for 3 h. This figure is available in colour online at www.interscience.wiley.com/journal/jrs.

or AgI , Ag_2S and Ag_2Se) are widely known as *solid electrolyte glasses*. They form homogeneous glasses displaying a single glass transitions, but exceptions occur. That result in itself is quite surprising although it has never been addressed satisfactorily in the literature. Solid electrolyte glasses have attracted much interest as sensors, as materials for battery applications and in flat panel displays.⁶⁰ The electrical conductivity of these materials can be increased by several orders of magnitude by alloying with increasing amounts of a solid electrolyte additive, but quantitative details are sparse.⁶¹ Recently, it was recognized⁶² that alloys of AgI and Ag_2Se can exist in a fast-ion-conducting glassy phase. Their T_g 's were established in m-DSC experiments and the results rationalized in terms of their global connectivity on the basis of constraint-counting algorithms. Recently Novita and Boolchand,⁶³ and separately Holbrook *et al.*,⁶⁴ have observed reversibility windows in two prototypical oxide- and chalcogenide-based solid electrolyte glass systems, respectively. Furthermore, they have found that sharp thresholds for ionic conduction coincide with the three elastic phases of glassy networks. Activation energies for ionic conduction ΔE_A decrease sharply when glasses enter the IP from the stressed-rigid and, furthermore, when the rigid glasses become flexible. These results open a new paradigm in the study of electric transport in solid electrolyte glasses.

m-DSC results on dry $(\text{AgPO}_3)_{1-x}(\text{AgI})_x$ glasses⁶⁵ show glass transition temperatures to steadily decrease as the AgI content of the glasses increases. This is in harmony with the low effective connectivity of AgI glass as discussed earlier.⁶² Previous work in the field^{61,66} has also found such compositional trends in the present AgPO_3 - AgI glasses except that the reported T_g 's are almost 50 to 80°C lower than the ones found by Novita *et al.*⁶⁵ The difference can be traced to the presence of bonded water in these glasses that lowers the connectivity, and therefore T_g , of the glasses. The central finding of the m-DSC is the observation of a broad reversibility window in the $9.5\% < x < 37.8\%$ AgI range, which, in analogy with chalcogenide glasses,⁴⁻⁹ fixes the three elastic phases: glasses in the $0 < x < 9.5\%$ range are viewed to be stressed-rigid, those in the $9.5\% < x < 37.8\%$ to be in the IP while those at $x > 38\%$ to be in the flexible phase. The room-temperature electrical conductivity of these glasses also has a threshold near $x = 9.5\%$ and a second one near $x = 37.8\%$, the elastic phase boundaries suggested by the thermal measurements.

Raman scattering again provides important clues on the molecular structure of these glasses. Figure 11 captures the observed lineshape of the base AgPO_3 glass. It is dominated by two modes, one near 684 cm^{-1} and the other near 1140 cm^{-1} . The base AgPO_3 glass is widely recognized to be composed of chains of PO_3 units (or Q^2 units in NMR notation) having two bridging (O_b) and two terminal (O_t) oxygens near-neighbors of P. Here Q^n represents the number of P cations that have n bridging oxygen near-neighbors. The modes near 1140 cm^{-1} (PO_t) and 684 cm^{-1} (PO_b) are

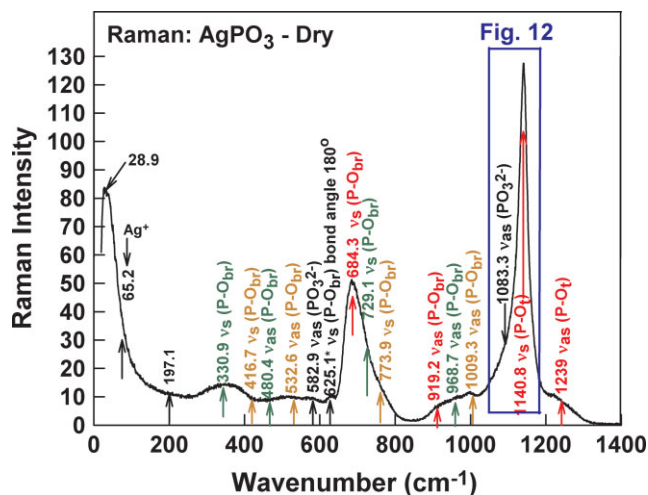


Figure 11. Raman scattering of a dry AgPO_3 base glass (taken from Ref. 63) displaying several vibrational modes whose assignments are indicated in the figure. This figure is available in colour online at www.interscience.wiley.com/journal/jrs.

characteristic of polymeric chains made of PO_3 units. With increasing AgI content, one observes a systematic evolution of modes; chain mode strength steadily goes over into ring modes of both small and large size. Assignment of the ring modes is facilitated by the tetrameric form⁶⁷ of $c\text{-AgPO}_3$ and other reference crystalline phosphates where large rings are manifested.⁶⁸ The central message contained in the Raman results is that there is a morphological transition in glass structure from polymeric at low x ($<25\%$) to monomeric as $x > 30\%$. AgI additive serves to decouple the network of chains by steadily inserting itself between chains at low x , and converting long chains to closed rings at high x . These observations are broadly consistent with the earlier MD simulations⁶⁹ and molar volume results.⁷⁰ In the MD simulations, a conductivity percolation transition was predicted near $x \sim 0.3$, which is consistent with the conductivity increase observed in these glasses. However, the observation of an IP in these glasses suggests that mean-field descriptions⁶⁹ of these glasses are unlikely to correctly get the details of these compositional trends in conductivity.

Of special interest is the vibrational mode near 1140 cm^{-1} , which is associated with P-O_t bonds in long chains. Through the two terminal oxygen near-neighbors in PO_3 this particular mode serves to probe the connectedness of the AgI-modified AgPO_3 base glass network. As the P-O-P chain spacings in the base glass (AgPO_3) increase upon AgI alloying, the wavenumber of the P-O_t mode steadily red shifts (Fig. 12). It therefore plays a role that is analogous to that of the CS GeSe_4 mode in binary Ge-Se glasses. Since the mode is rather well resolved in the Raman spectra (Fig. 12), one can analyze the lineshapes and extract the compositional variation of the mode wavenumber quite accurately. The mode wavenumber displays two distinct thresholds, one near $x = 9.5\%$ and another near

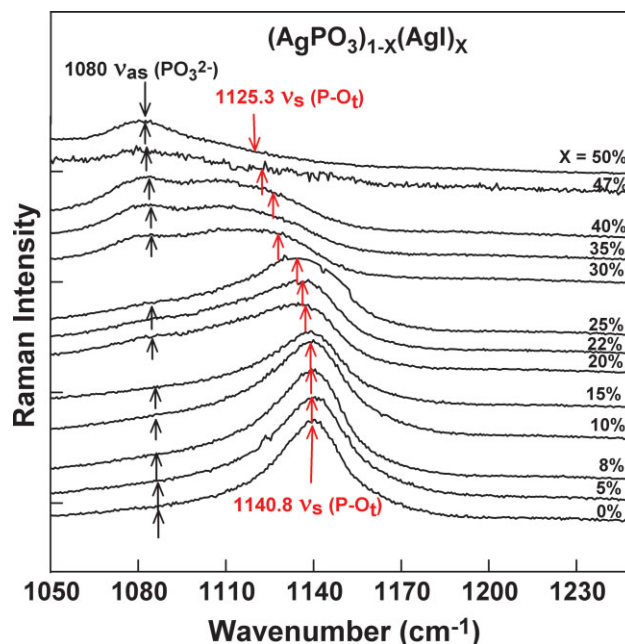


Figure 12. Raman spectra of $(\text{AgPO}_3)_{1-x}(\text{AgI})_x$ glasses showing a red shift of the symmetric PO_t mode of long chains with increasing AgI content. The shift shows that the network steadily softens as the interchain spacings increase. This figure is available in colour online at www.interscience.wiley.com/journal/jrs.

$x = 37.8\%$. Furthermore, the wavenumber optical elasticity power laws in the $0 < x < 9.5\%$ range and in the $9.5\% < x < 37.8\%$ range, can also be established, and their values are found to be characteristic of those of stressed-rigid and IP glasses found in the covalently bonded networks. These new findings on solid electrolytes will be presented in a forthcoming publication.⁶⁵ These results open a new paradigm to understand fast ion transport in terms of the elastic response of their networks. For the purpose of this review, these findings serve to illustrate the usefulness of Raman scattering as an elegant probe of IPs in disordered networks through measurements of *optical elasticity power laws*.

CONCLUSIONS

The discovery of IPs has opened new vistas in understanding the disordered state of condensed matter.^{4,7,13,21} In this review we have illustrated applications of Raman scattering as a probe of the elastic phases in glassy networks, and in particular in characterizing IPs by their optical elasticity power laws. Three types of material systems were considered: a chalcogenide bulk glass, a chalcogenide amorphous thin film and a solid electrolyte bulk glass. IP glassy networks are rather special because they form ideal, space-filling, and stress-free networks, with unusual functionalities. Absence of aging, giant PC in obliquely

deposited chalcogenide films and a pronounced increase in electrical conductivity represent some of the functionalities displayed by IP glasses in the three examples chosen here. Disordered glassy networks form over a very small part of composition phase space, and IP glasses select an even smaller part of that phase space in which the glass-forming tendency is optimized. This is in contrast with amorphous networks rendered disordered by virtue of synthesis, such as vapor deposition onto cold substrates, which may or may not display a glass transition. Amorphous thin films of IP glass compositions in the Ge–Se binary also appear to display unusual functionalities; they form a columnar structure that can undergo facile photocollapse accounting for the giant PC observed in these films. IPs have now been identified^{21,24,25} in numerical simulations on triangular networks in 2D, and their physical properties including the feature of self-organized criticality are being explored further. As these investigations evolve, a better understanding of the structural features at a local and medium-range scale, which endow these systems with their unusual functionalities, can be expected to emerge. Window glass is an example of a self-organized oxide glass network whose chemical composition can now be derived rather accurately from two basic principles of aggregation and structure.¹⁰ The importance of these generic elastic phases of disordered networks also has significant consequences in protein science.¹² They are beginning to assist in understanding the pathways taken by proteins when they fold and unfold reversibly. IP glasses most likely represent the ultimate self-organized nanostructured functional materials optimized by nature.

Acknowledgements

We have benefited from ongoing discussions with J. C. Phillips, Ping Chen, B. Goodman, D. McDaniel, S. Mamedov and M. Micoulaut. This work is supported by NSF grants DMR-04-56472 and IMR-0315491.

REFERENCES

- Kauzmann W. *Chem. Rev.* 1948; **43**: 219.
- Phillips JC. *J. Non-Cryst. Solids* 1979; **34**: 153.
- Feng XW, Bresser WJ, Boolchand P. *Phys. Rev. Lett.* 1997; **78**: 4422.
- Boolchand P, Georgiev DG, Goodman B. *J. Optoelect. Adv. Mater.* 2001; **3**: 703.
- Selvanathan D, Bresser WJ, Boolchand P. *Phys. Rev., B* 2000; **61**: 15061.
- Qu T, Georgiev DG, Boolchand P, Micoulaut M. In *Supercooled Liquids, Glass Transition and Bulk Metallic Glasses*, vol. 754, Egami T, Greer AL, Inoue A, Ranganathan S (eds). Materials Research Society Symposium Proceedings, Warrendale, PA, 2003; 111.
- Chakravarty S, Georgiev DG, Boolchand P, Micoulaut M. *J. Phys.-Condens. Matter* 2005; **17**: L1.
- Boolchand P, Feng X, Bresser WJ. *J. Non-Cryst. Solids* 2001; **293**: 348.
- Wang Y, Wells J, Georgiev DG, Boolchand P, Jackson K, Micoulaut M. *Phys. Rev. Lett.* 2001; **87**: 185503.
- Kerner R, Phillips JC. *Solid State Commun.* 2000; **117**: 47.
- Lucovsky G, Phillips JC. *J. Non-Cryst. Solids* 1998; **230**: 1221.
- Rader AJ, Hesperheide BM, Kuhn LA, Thorpe MF. *Proc. Natl. Acad. Sci. U.S.A.* 2002; **99**: 3540.
- Boolchand P, Lucovsky G, Phillips JC, Thorpe MF. *Philos. Mag.* 2005; **85**: 3823.
- Lagrange JL. *Mechanique Analytique*. Desaint: Paris, 1788.
- Maxwell JC. *Philos. Mag.* 1864; **27**: 294.
- Thorpe MF. *J. Non-Cryst. Solids* 1983; **57**: 355.
- Kamitakahara WA, Cappelletti RL, Boolchand P, Halfpap B, Gompf F, Neumann DA, Mutka H. *Phys. Rev., B* 1991; **44**: 94.
- He H, Thorpe MF. *Phys. Rev. Lett.* 1985; **54**: 2107.
- Franzblau DS, Tersoff J. *Phys. Rev. Lett.* 1992; **68**: 2172.
- Thorpe MF, Jacobs DJ, Chubynsky MV, Phillips JC. *J. Non-Cryst. Solids* 2000; **266**: 859.
- Thorpe MF, Chubynsky MV. In *Phase Transitions and Self-Organization in Electronic and Molecular Networks*, Phillips JC, Thorpe MF (eds). Kluwer Academic/Plenum Publishers: Cambridge, 2000; 43.
- Wang F, Mamedov S, Boolchand P, Goodman B, Chandrasekhar M. *Phys. Rev., B* 2005; **71**: 174201.
- Micoulaut M, Phillips JC. *Phys. Rev., B* 2003; **67**: 104204.
- Barre J, Bishop AR, Lookman T, Saxena A. *Phys. Rev. Lett.* 2005; **94**: 208701.
- Briere M-A, Chubynsky MV, Mousseau N. <http://arxiv.org/abs/cond-mat/0610557> [2006].
- Yu P, Cardona M. *Fundamentals of Semiconductors*. Springer-Verlag: Berlin, 1996.
- Raman CV. *Nature* 1919; **103**: 165.
- Zallen R. *The Physics of Amorphous Solids*. Wiley: New York, 1983.
- Zallen R. *Phys. Rev., B* 1974; **9**: 4485.
- Murase K, Fukunaga T. In *Optical Effects in Amorphous Semiconductors*, Taylor PC, Bishop SG (eds). American Institute of Physics: New York, 1984; 449.
- Brillouin L. *Phys. Rev.* 1938; **54**: 916.
- Gump J, Finkler I, Xia H, Sooryakumar R, Bresser WJ, Boolchand P. *Phys. Rev. Lett.* 2004; **92**: 245501.
- Vaills Y, Qu T, Micoulaut M, Chaimbault F, Boolchand P. *J. Phys.-Condens. Matter* 2005; **17**: 4889.
- Birge NO, Nagel SR. *Phys. Rev. Lett.* 1985; **54**: 2674.
- Modulated DSC Compendium, Reprint #TA 210*. T.A. Instruments, Inc: New Castle, DE, 1997; (<http://www.tainstruments.com>).
- Boolchand P, Georgiev DG, Micoulaut M. *J. Optoelect. Adv. Mater.* 2002; **4**: 823.
- Weeks ER, Crocker J, Levitt AC, Schofield A, Weitz D. *Science* 2000; **287**: 627.
- Kerner R, Micoulaut M. *J. Non-Cryst. Solids* 1997; **210**: 298.
- Boolchand P, Georgiev DG, Qu T, Wang F, Cai LC, Chakravarty S. *Compt. Rendus Chim.* 2002; **5**: 713.
- Boolchand P. *Asian J. Phys.* 2000; **9**: 709.
- Chakravarty S. MS Thesis, University of Cincinnati, 2003.
- Zallen R, Lucovsky G. In *Selenium*, Zingaro R, Cooper W (eds). Van Nostrand Reinhold: New York, 1974; 170.
- Jackson K, Briley A, Grossman S, Porezag DV, Pederson MR. *Phys. Rev., B* 1999; **60**: R14985.
- Bridenbaugh PM, Espinosa GP, Griffiths JE, Phillips JC, Remeika JP. *Phys. Rev., B* 1979; **20**: 4140.
- Georgiev DG, Boolchand P, Micoulaut M. *Phys. Rev., B* 2000; **62**: R9228.
- Verrall DJ, Elliott SR. *Phys. Rev. Lett.* 1988; **61**: 974.
- Choi S, Han S, Wang S. *Thin Solid Films* 2002; **413**: 177.
- Lannin J, Shanabrook B. *Solid State Commun.* 1978; **28**: 497.
- Venkateswaran C. *Proc. Acad. Sci.* 1935; **Sect. A2**: 260.
- Andreas K, Alexander K, Martin T. *J. Chem. Phys.* 2002; **116**(8): 3323.
- Cobb M, Drabold DA, Cappelletti RL. *Phys. Rev., B* 1996; **54**: 12162.

52. Wang F, Boolchand P, Jackson K, Micoulaut M. 2006 (submitted).
53. Singh B, Rajagopalan S, Bhat PK, Pandya DK, Chopra KL. *J. Non-Cryst. Solids* 1980; **35–36**: 1053.
54. Chopra KL, Harshvardhan KS, Rajagopalan S, Malhotra LK. *Solid State Commun.* 1981; **40**: 387.
55. Phillips JC, Cohen ML. *Phys. Rev., B* 1982; **26**: 3510.
56. Dirks AG, Leamy HJ. *Thin Solid Films* 1977; **47**: 219.
57. Jin M, Chen P, Boolchand P, Rajagopalan S, Chopra KL. (unpublished).
58. Lucovsky G, Nemanich RJ, Galeener FL. In *Center for Industrial Consultancy and Liason*, Spear WE (ed.). University of Edinburgh: Dundee, 1977; 130.
59. Fritzsche H. *Insulating and Semiconducting Glasses*, Boolchand P (ed.). World Scientific: Singapore, River Edge, 2000; xi.
60. Angell C. *Annu. Rev. Phys. Chem.* 1992; **43**: 693.
61. Sidebottom L. *J. Phys.: Condens. Matter* 2003; **15**: S1585.
62. Boolchand P, Bresser WJ. *Nature* 2001; **410**: 1070.
63. Novita DI, Boolchand P. IEEE Nano 2006. In *6th IEEE Conference on Nanotechnology*, Cincinnati, OH, 2006 (in press).
64. Holbrook C, Chen P, Novita DI, Boolchand P. IEEE Nano 2006. In *6th IEEE Conference on Nanotechnology*, Cincinnati, OH, 2006 (in press).
65. Novita DI, Fayon F, Malki M, Micoulaut M, Boolchand P. (unpublished).
66. Kartini E, Collins MF, Priyanto T, Yusuf M, Indayaningsih N, Svensson EC, Kennedy SJ. *Phys. Rev., B* 2000; **61**: 1036.
67. Rulmont A, Cahay R, Liegeois-Duyckaerts M, Tarte P. *Eur. J. Solid State Inorg. Chem.* 1991; **28**: 207.
68. Simon VA, Steger E. *Z. anorg. Allg. Chemie.* 1954; **277**(5): 209.
69. Wicks JD, Börjesson L, Bushnell-Wye G, Howells WS, McGreevy RL. *Phys. Rev. Lett.* 1995; **74**: 726.
70. Swenson J, Borjesson L. *Phys. Rev. Lett.* 1996; **77**: 3569.